Science Bulletin 64 (2019) 180–188

Contents lists available at ScienceDirect

Science Bulletin

journal homepage: www.elsevier.com/locate/scib

Article

Tauroursodeoxycholic acid (TUDCA) inhibits influenza A viral infection by disrupting viral proton channel M2

Ning Li [a,1,2], Yanxu Zhang [a,1], Shuangxiu Wu [a,1], Ruodan Xu [b], Zhiqing Li [a], Jindong Zhu [a], Hongliang Wang [a], Xiao Li [c], Mingyao Tian [c], Huijun Lu [c], Ningyi Jin [c,*], Chengyu Jiang [a,*]

[a] State Key Laboratory of Medical Molecular Biology, Institute of Basic Medical Sciences, Chinese Academy of Medical Sciences, Peking Union Medical College, Tsinghua University, Beijing 100005, China
[b] Interdisciplinary Nanoscience Center (iNANO), Department of Engineering, Aarhus University, 8000 Aarhus C, Denmark
[c] Genetic Engineering Laboratory, Institute of Military Veterinary, Academy of Military Medical Sciences, Changchun 130062, China

ARTICLE INFO

Article history:
Received 26 March 2018
Received in revised form 22 June 2018
Accepted 22 July 2018
Available online 1 September 2018

Keywords:
Influenza
TUDCA
M2 proton channel
Virus entry
Cell-penetrating peptide
Oligomerization inhibitor

ABSTRACT

Influenza is a persistent threat to human health and there is a continuing requirement for updating anti-influenza strategies. Initiated by observations of different endoplasmic reticulum (ER) responses of host to seasonal H1N1 and highly pathogenic avian influenza (HPAI) A H5N1 infections, we identified an alternative antiviral role of tauroursodeoxycholic acid (TUDCA), a clinically available ER stress inhibitor, both *in vitro* and *in vivo*. Rather than modulating ER stress in host cells, TUDCA abolished the proton conductivity of viral M2 by disrupting its oligomeric states, which induces inefficient viral infection. We also showed that M2 penetrated cells, whose intracellular uptake depended on its proton channel activity, an effect observed in both TUDCA and M2 inhibitor amantadine. The identification and application of TUDCA as an inhibitor of M2 proton channel will expand our understanding of IAV biology and complement current anti-IAV arsenals.

1. Introduction

As major human pathogens, influenza A viruses (IAV) continuously induce annual outbreaks and irregular epidemics [1]. The highly pathogenic avian influenza (HPAI) A H5N1 is one plausible candidate that can cause deadly flu outbreak [2]. Though the basis for the incremental virulence of H5N1 is largely unclear, clinical data suggest high viral load and the resulting cytokine storm are primary instigating factors [3]. Therefore, identifying therapies that target viral elements involved in different steps of IAV life cycle remains a public health priority [3].

Life cycle of enveloped IAV initiates from receptor-mediated endocytosis, inhibition of which presents an ideal approach to restrict IAV replication and spread [4]. Dynamic entry of IAV starts from binding of haemagglutinin (HA) with sialic acid [5], followed by two pH-controlled events. The optimal acid milieu in late endosomes triggers conformational alterations of HA, which fuses IAV with host endosomal membrane. Prior to fusion, acidic activation of the M2 ion channel occurs in early endosomes, which facilitates IAV uncoating [6]. Thus, inhibiting HA or M2 constitutes the primary mechanisms to suppress IAV entry. Though M2 inhibitors, amantadine and rimantadine, can block IAV entry, the emergence of adamantane-resistant M2 and associated adverse effects temper their clinical application [7].

M2 is a homo-tetramer, and each monomer consists of 97 amino acids, including an ectodomain, a transmembrane (TM) region and a cytosolic tail containing an amphipathic α-helix (AH) [8]. M2 proton conduction may involve interactions between protonated His37 and Trp41 of TM at an acidic pH, which is responsible for adamantane-based sensitivity [9]. M2 oligomerization, based on assessment of either tetramerization of M2 TM peptides or dimerization of full-length M2, was particularly necessary for its entire channel function [8–11]. TM of M2 was sufficient to form tetrameric M2 [12], which was unstable unless AH is present [9,10,13]. Though M2 structural conformation and function remains unclear [10,14–17], deforming oligomeric M2 will pave the way for the development of anti-IAV drugs.

Bile acids (BA) are amphipathic molecules composed of a hydrophobic backbone and hydrophilic hydroxyl groups [18]. BA are usually conjugated with taurine to increase hydrophilicity. BA-based medications have evolved from hydrophobic chenodeoxycholic acid (CDCA) and its taurine-conjugate TCDCA to more

* Corresponding authors.
E-mail addresses: Ningyik@126.com (N. Jin), Jiang@pumc.edu.cn (C. Jiang).
[1] Authors contributed equally.
[2] Present address: China Academy of Chinese Medicine Sciences, Beijing 100700, China.

https://doi.org/10.1016/j.scib.2018.08.013
2095-9273/

hydrophilic ursodeoxycholic acid (UDCA) and its taurine-conjugate TUDCA. Both later strategies are current FDA-approved treatments for human liver disorders [19]. Since BA reduces intracellular protein aggregates as chaperone 4-phenylbutyrate (4-PBA) does, UDCA and TUDCA are considered as chemical chaperones [20]. Recently, TUDCA is implicated as a therapy for hepatitis B virus infection [21]. TUDCA also inhibits IAV replication [22] by suppressing the inositol-requiring enzyme 1 (IRE1) branch of the unfolded protein response (UPR) [22,23], a conserved molecular network orchestrating ER pathology.

In our current study, we observed distinct ER responses to seasonal H1N1 and highly pathogenic H5N1 infections in lung epithelium. Though lack of typical UPR signaling, the ER stress inhibitor TUDCA is sufficient to prevent H5N1-induced lung injuries in an UPR independent manner. Our results show that disrupting the M2 proton channel may account for TUDCA inhibition of IAV infection.

2. Materials and methods

2.1. Cell lines

Human lung adenocarcinoma (A549) cell lines were obtained from ATCC. Madin-Darby canine kidney (MDCK) and human embryonic kidney (HEK293T) cells were purchased from Cell Resource Centre of Peking Union Medical College (Beijing, China). Details are given in Supplemental Experimental Procedures.

2.2. Influenza viruses, virus propagation and animal infection

Avian influenza virus A/Jilin/9/2004 (H5N1) and seasonal influenza virus A/New Caledonia/20/1999 (H1N1) used in this study were obtained by inoculating stock virus into 10-day old specific-pathogen-free (SPF) embryonated chicken eggs and harvested from allantoic fluid (AF) of eggs. For animal infection, SPF-housed C57BL/6J mice (4-week old, male, 16–18 g) from Vital River (Beijing, China) were used and infected. Lung injury was induced by intratracheal injection of live H5N1 IAV at a titre of 1×10^6 $TCID_{50}$-1.6×10^6 $TCID_{50}$ or identical volume of AF (vehicle control). Body weight and survival rate were recorded every day after intratracheally challenged with either AF or H5N1 IAV. TUDCA at 150 mg/kg was intratracheally administrated to mice 24 and 6 h before IAV exposure or 6 and 24 h after IAV injection to determine prophylactic and therapeutic effects, respectively. Dose of TUDCA for in vivo tests was chosen from previous studies [20]. Histological assessment of mouse lung tissue and measurement of mouse lung wet/dry ratio were performed 4 days post infection. Lung injury scores were fulfilled as described [24]. Details are given in Supplemental Experimental Procedures. All applicable institutional and/or national guidelines for the care and use of animals were followed.

2.3. Experiments with iVLP

IVLPs were obtained by transfection of HEK293T cells with plasmids encoding IAV elements. IVLP-based M2 proton channel activity was measured by modifying previously published protocols [25]. Details are given in Supplemental Experimental Procedures.

2.4. Flow cytometry and immuno-blotting

Quantification of intracellular iVLP was determined by Accuri C6 Flow Cytometer (Becton Dickinson, BD, Franklin Lakes, NJ, USA) and analyzed using FlowJo software (TreeStar, Ashland, OR, USA). Corresponding antibodies and details are in Supplemental Experimental Procedures.

2.5. Experiments with microscope

Confocal images, including those with acid bypass tests, were acquired using an Olympus FV1000 confocal microscope (FV-1000, Olympus, Tokyo, Japan). Quantification of signals was performed with Olympus Fluoview 3.0 (Olympus). Negative staining of iVLP and observation of infected A549 cells were performed with transmission electron microscope (JEM 1230, JEOL, Tokyo, Japan). Details are given in Supplemental Experimental Procedures.

2.6. Statistics

All data shown are mean ± SEM, analyzed according to at least 3 independent experiments. Two-group comparison was analyzed by student's *t*-test, and statistical tests of multiple groups were performed by ANOVA followed by Turkey post-test with IBM SPSS 19.0 or GraphPad Prism 5.0 (San Diego, CA, USA). $P < 0.05$ was considered as statistically significant.

3. Results

3.1. Different ER responses to seasonal H1N1 and highly pathogenic H5N1 infection

Previous studies showed that TUDCA constrained seasonal PR/8/34 H1N1 IAV-induced UPR in lung epithelium [22]. We consistently observed increased IRE-1α and Bip signals of UPR in A549 cells after infection with seasonal New Caledonia/20/1999 H1N1 IAV (Fig. S1a online). UPR activation occurred in parallel with hyperplasia of smooth ER, which became striking 24 h post infection (Fig. 1a). However, UPR responsive pathways were absent in HPAI A H5N1-challenged host (Fig. S1b online), including IRE-1α branch (Fig. S1a online). Though lack of typical UPR signatures, a remarkable ER swelling was detectable 1 h after H5N1 infection (Fig. 1a). This result confirmed ER involvement in IAV life cycle and further suggested different ER responses to seasonal and highly pathogenic IAV infection. In contrast to previous reports where UPR activation mediates pandemic IAV-induced acute lung injuries (ALI) [23], the absence of UPR in highly pathogenic H5N1-infected cells in our study suggests alternative underlying mechanisms. In light of severe ER swelling induced 1 h after H5N1 infection, we explored the potentiality of clinically available ER stress inhibitors, TUDCA and 4-PBA, as anti-H5N1 strategies.

3.2. TUDCA protects the host against H5N1 IAV infection independent of UPR

To investigate anti-H5N1 actions of ER chaperones, we first tested the effects of TUDCA in H5N1-infected cells. When added 12 h before and during infection, TUDCA restored A549 cell viability from 41.6% to 82.5% 48 h after H5N1 exposure (Fig. 1b) with a nearly undetectable viral load (Fig. 1c). Notably, the anti-H5N1 effect of TUDCA was only achieved at relatively high doses, which were much greater than those used to relieve ER stress [22,23]. In view of good tolerance and apparent benefits of high dose TUDCA against lethal IAV infection (Fig. S1c, d online), we utilized 3 mmol/L in our in vitro studies. Due to lack of UPR, TUDCA did not impact UPR markers in H5N1-exposed cells, though H1N1-infected cells could possess a tight association of TUDCA with IRE-1α (Fig. S1a, b online), as shown previously [22]. In contrast, 4-PBA failed to rescue H5N1-induced cell death (Fig. S1e, f online), which supports an UPR-independent antiviral action of TUDCA. Moreover, protection

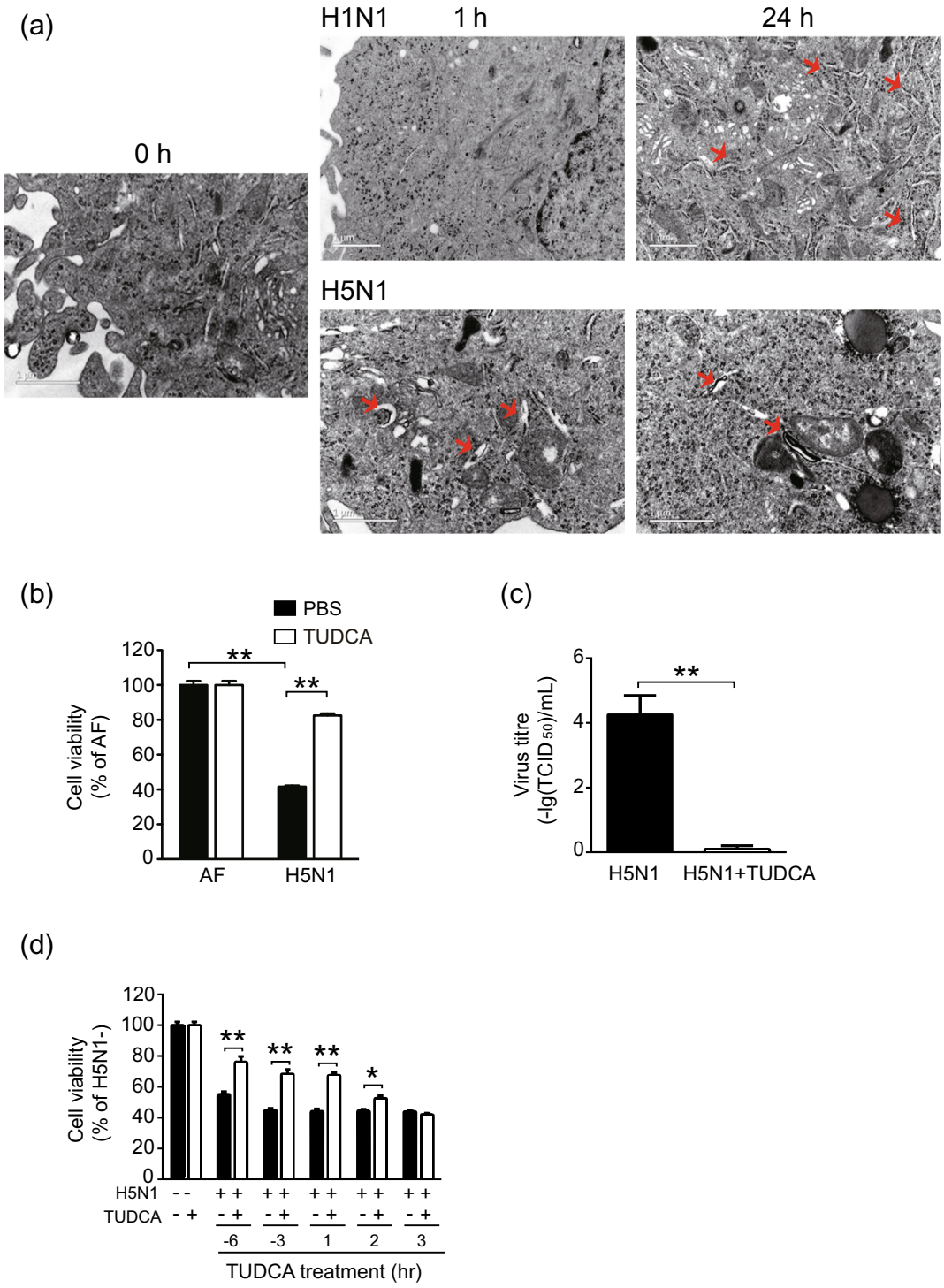

Fig. 1. Different ER morphologies after IAV infection and effects of TUDCA. (a) TEM data from A549 cells 1 and 24 h after H1N1 or H5N1 IAV infection compared to non-infected (0 h). (b) A549 cell viability measured 48 h after H5N1 IAV infection compared with non-infected AF controls in the absence (PBS) or presence of TUDCA. (c) Virus titre measured in MDCK cells to evaluate viral load (b) 12 h post infection. (d) Prophylactic and therapeutic efficacy of TUDCA in H5N1-infected A549 cells. Prophylactically, TUDCA was added 6 or 3 h prior to and concomitant with H5N1 exposure. Therapeutically, TUDCA was given 1, 2 or 3 h after H5N1 infection. *, $P \leq 0.05$ and **, $P \leq 0.01$.

of the host against H5N1 infection was unsuccessful when TUDCA was added 3 h post H5N1 challenge compared to prophylactic interventions (−6 and −3 h) or therapeutic treatments within 2 h after infection (Fig. 1d). As 2–3 h is the critical time point corresponding to the end of HA fusion and the start of viral genome transportation [26], our results suggest IAV entry as a target of TUDCA.

3.3. TUDCA targets IAV entry

To examine the anti-entry role of TUDCA, we quantified internalized H5N1 IAV 1 and 3 h post infection (Fig. 2a, S2a). In infected cells, NP positive staining was 1.5% and 16.7% of the total cell area after 1 and 3 h of H5N1 infection, respectively. TUDCA reduced about 90% NP signals at both 1 and 3 h post infection. Of note,

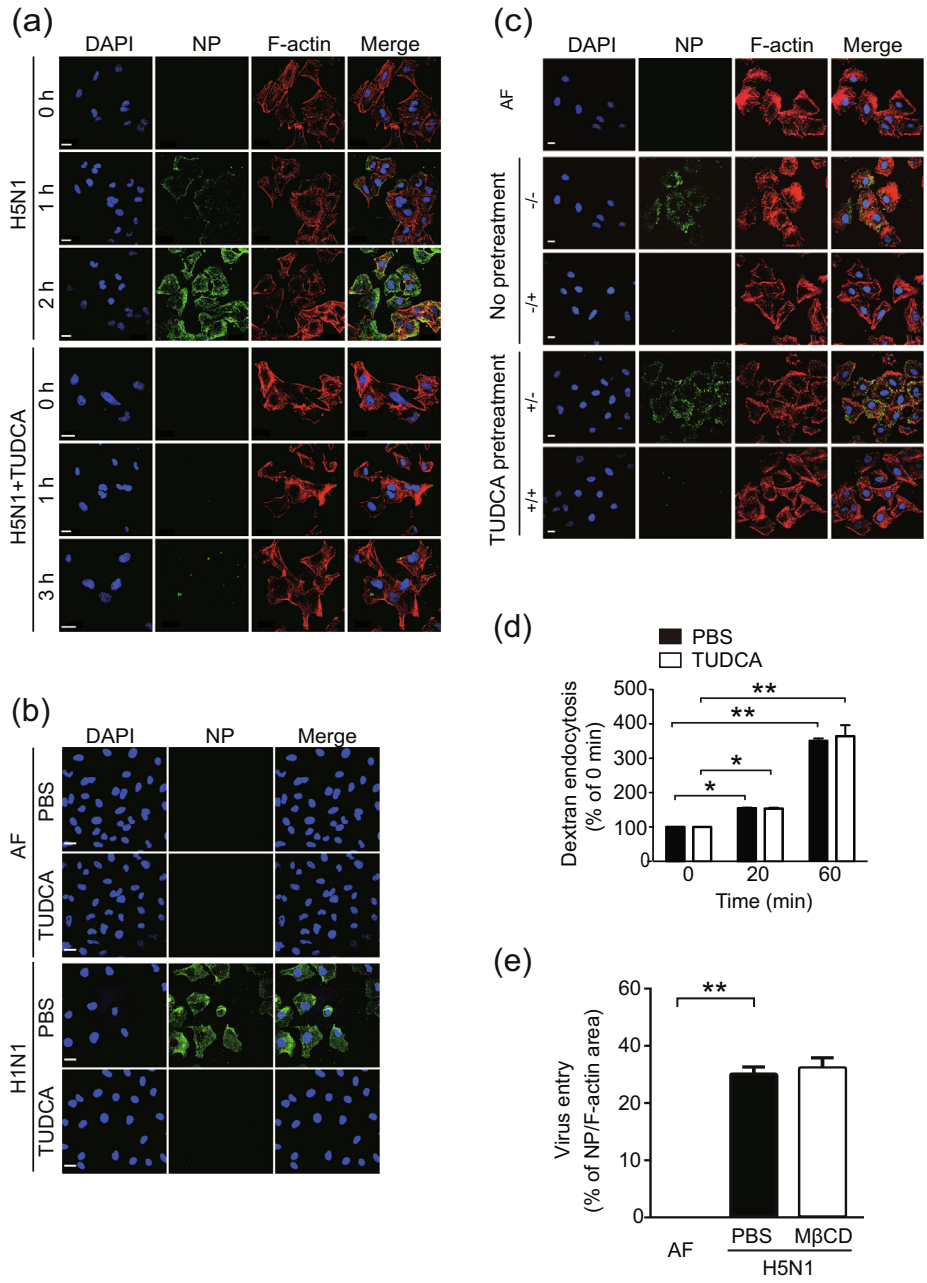

Fig. 2. TUDCA targets IAV elements involved in entry. (a, b) Confocal observations of internalized H5N1 (a) and H1N1 (b, 3 h) IAV. (c) Permutations of TUDCA treatments according to whether TUDCA exists prior to or concomitant with H5N1 infection, compared with non-infected and non-treated control (AF). Green: NP, Red: F-actin and Blue: nuclei stained with DAPI, scale bar: 20 μm. (d) Dextran uptake into A549 cells in the presence or absence (PBS) of TUDCA. (e) Effects of MβCD-pretreated A549 cells on H5N1 IAV internalization. *, $P \leq 0.05$ and **, $P \leq 0.01$.

blockage of IAV entry by TUDCA was not exclusive to H5N1, as we found a similar 90% suppression of IAV entry in cells infected with H1N1 (Figs. 2b and S2b (online)). Altogether, these results provide evidence that TUDCA inhibits IAV entry.

3.4. TUDCA interferes with IAV

Mechanisms of IAV entry reflect the interplay between IAV and host endocytic machineries. To clarify in which step TUDCA plays a role, we permuted TUDCA treatment into four tactics based on when TUDCA is administered to the host, namely either before or concomitant with IAV infection (Figs. 2c and S2c (online)). Intriguingly, even when cells were not pre-exposed, as long as TUDCA was applied during IAV infection (−/+), TUDCA inhibition of IAV entry was comparable to the condition where TUDCA was added both before and during infection (+/+). Meanwhile, presence of TUDCA during infection (−/+ and +/+) was critical, as removal of TUDCA during infection even after a 12 h pre-treatment of the host (+/−) failed to prevent viral infection, an effect similar to non-TUDCA-treated cells (−/−). This result suggests that the anti-IAV effects of TUDCA unlikely rely on priming host cells. We further verified this point by testing dynamics of host cell endocytosis using virus-free, fluorescence-labeled dextran (Fig. 2d). Our results showed no inhibition of dextran uptake by TUDCA at both 20 and 60 min after dextran loading, indicating that TUDCA does not affect host endocytosis. In addition, TUDCA as a bile acid may sequester

cholesterol from the cellular membrane, leading to attenuated viral entry [27]. Here, we found no decrease of internalized H5N1 when cells were pre-incubated with cholesterol-depleting methyl-β-cyclodextrin (MβCD, Figs. 2e and S2d (online)), consistent with H1N1-infected cells [28]. Altogether, these data indicate TUDCA may target IAV instead of the host.

3.5. TUDCA disrupts M2

As HA mediates both receptor-binding and acid-controlled fusion during IAV entry, we tested the effects of TUDCA on HA using the acid bypass assay [6]. Briefly, acid bypass mimics the acidic environment of late endosomes in the extracellular compartment, which deceives the viral HA expose fusion-peptide without allocation in late endosomes. In response to acid, the pre-attached IAV should immediately fuse with the plasma membrane. As shown in Fig. 3a, inhibition of TUDCA on IAV internalization was completely abolished when acid bypass was applied, suggesting that TUDCA does not interfere with receptor-binding and fusion of HA.

To gain deeper insight into other individual elements of the IAV envelope, we utilized the influenza virus-like particles (iVLPs). Since M1 is essential for efficient iVLPs assembly, we created iVLPs containing HA, NA and M1 (iVLPhnm1), M1 and M2 (iVLPm1–2) or HA, NA, M1 and M2 (iVLP4, Fig. S3a, b online). We then determined entry of iVLPs in A549 cells (Figs. 3b and S3c–e (online)). Our results showed that TUDCA had minor effects on iVLPhnm1 uptake. However, TUDCA interrupted the internalization iVLPm1–2, even in the absence of fusion protein HA (Fig. 3b).

To gain insight into the mechanism by which TUDCA suppresses iVLPm1–2 cell-penetration, we tested whether iVLPm1–2 was internalized via an endocytic pathway. By employing bafilomycin A1 and chloroquine (CQ), we observed elevated iVLPm1–2 signals in A549 cells (Fig. S3e online). This pattern indicates a deficiency in degrading engulfed iVLPm1–2, suggesting endocytosis as a mechanism for iVLPm1–2 entry into cells.

To clarify which components of iVLPm1–2 determine its cell-penetration, we utilized mammalian-cell derived M1 or M2 protein to treat A549 cells. In cell-based experiments, we did not detect any endocytosed M1 in A549 cells; however, M2 from both H5N1 and H1N1 IAV could be clearly detected, which was attenuated by TUDCA (Figs. 3b and S3h (online)). Together with inhibition of iVLPm1–2 uptake by M2 inhibitor amantadine (Fig. 3b), it is likely that entry of iVLPm1–2 is M2-dependent.

Moreover, co-incubating TUDCA with iVLPm1–2 revealed that M2 dimer and tetramer, especially tetramer, were lost when TUDCA was present, while HA, NA and M1 remained unaltered in all three iVLPs we created (Fig. 3c). We verified bands of M2 oligomers by M2 specific antibody (Fig. S3i online) and confirmed disruption of M2 oligomers by TUDCA through co-incubating TUDCA with either authentic H5N1 IAV (Fig. 3d) or corresponding iVLPm1–2 from A/Jilin/9/2004 strain (Fig. S3j online). Our results showed that TUDCA impaired M2 tetramer of both H5N1 IAV and iVLPm1–2 without an obvious impact on HA and M1 of authentic H5N1 IAV. Collectively, these data provide critical evidence that the effects of TUDCA are associated with M2.

Since the oligomeric stage of M2 may affect its channel activity [10], we then examined the proton conductivity of M2. Challenging iVLPm1–2 (Fig. 3e) or iVLP incorporated with Gag and M2 (iVLPgm2) [25] (Fig. S3k online) with acidic buffer resulted in membrane depolarization, an indication of M2 activation. In response to TUDCA injection, acid-stimulated proton translocation was largely abolished (Figs. 3e and S3k (online)), indicating M2 function requires oligomerization. However, amantadine or rimantadine treatment augmented tetrameric M2 (Fig. S3l online), suggesting a dissimilar mechanism of action of TUDCA.

Furthermore, using TEM we observed that iVLPm1–2 formed a liposome-like structure, which was distinctive from M1 and M2 protein alone. Consistent with endocytosis, M2 protein and iVLPm1–2, but not M1 protein, were dramatically disrupted after TUDCA addition (Fig. 3f), which was further confirmed by atomic forced microscopy (AFM, Fig. S3g online).

3.6. TUDCA ameliorates H5N1-induced ALI in vivo

Finally, we assessed whether TUDCA was a potential anti-IAV therapy. We tested the effect of TUDCA as both a prophylactic and a therapeutic approach. We administered prophylactic TUDCA or saline intraperitoneally in mice both 24 and 6 h before intratracheal challenge with H5N1 IAV. Similar to our *in vitro* data, TUDCA increased the survival rate of mice without detectable side effects (Fig. 4a). Reduced body weight in infected mice improved in TUDCA-treated subjects (Fig. 4b). Lung injury scores based on H&E staining (Fig. 4c) indicated a 50% reduction of lung impairment in TUDCA-treated mice (Fig. 4d), and pulmonary edema in infected mice dramatically recovered in TUDCA-treated groups (Fig. 4e). These results indicate that TUDCA is a highly effective prophylactic treatment against IAV-induced disease. Conversely, when TUDCA treatment began 6 and 24 h after H5N1 exposure, both survival rate and body weight in the TUDCA-treated group was indistinguishable from the non-treated group (Fig. S4a, b online). These in vivo observations confirm TUDCA targets internalization rather than replication of IAV.

4. Discussion and conclusion

The role of ER during IAV infection is well-documented [22,23], and the activation of UPR is not a unique feature of ER in IAV-infected cells [23]. Though mechanisms by which IAV induce ER stress have been attributed to accumulated IAV proteins in the ER lumen during IAV replication [22], changes of ER morphology 1 h post H5N1 exposure are indicative of other interactions between ER and IAV. Besides assembling and folding newly synthesized proteins, ER as intracellular bank of Ca^{2+} also regulates cytosolic Ca^{2+}. Indeed, IAV infection induced cytosolic Ca^{2+} oscillations in host cells, which was required for efficient IAV internalization [29]. Yet, details behind ER pathophysiology during IAV entry remain mostly unclear, it opens interesting questions – whether UPR activation induces detrimental or beneficial host responses following IAV infection and whether typical ER signals serve as indicators of viral virulence.

In the current study, we generated a series of iVLPs, among which iVLPm1–2 was of unexpected. First, it forms a liposome-like structure with measurable M2 proton channel activity. Second, iVLPm1–2 can penetrate freely into cells, probably through endocytic pathways. Third, the penetrating potential of iVLPm1–2 may rely on M2, which is likely endowed with a cell-penetrating competence. From the first identification of proteins that can move across cellular membranes, a group of proteins with similar features was classified as cell-penetrating peptides (CPPs) [30]. One class of CPPs was identified comprising a high degree of amphipathicity, where AH is the most common structural motif [31]. In AH, hydrophilic and hydrophobic amino acids are usually grouped on separate faces of helix, with a highly hydrophobic patch on one face and a cationic patch on the other face. Penetration of CPPs containing AH is mainly due to the amphipathicity of AH [32]. Regarding M2, the existence of AH in C-terminus has been reported by several groups [15,16,33] and its putative function involves viral budding and scission [33,34]. When expressed in host cells, AHs of M2, which are arranged parallel to membrane, partially penetrate themselves through its hydrophobic face mediating mem-

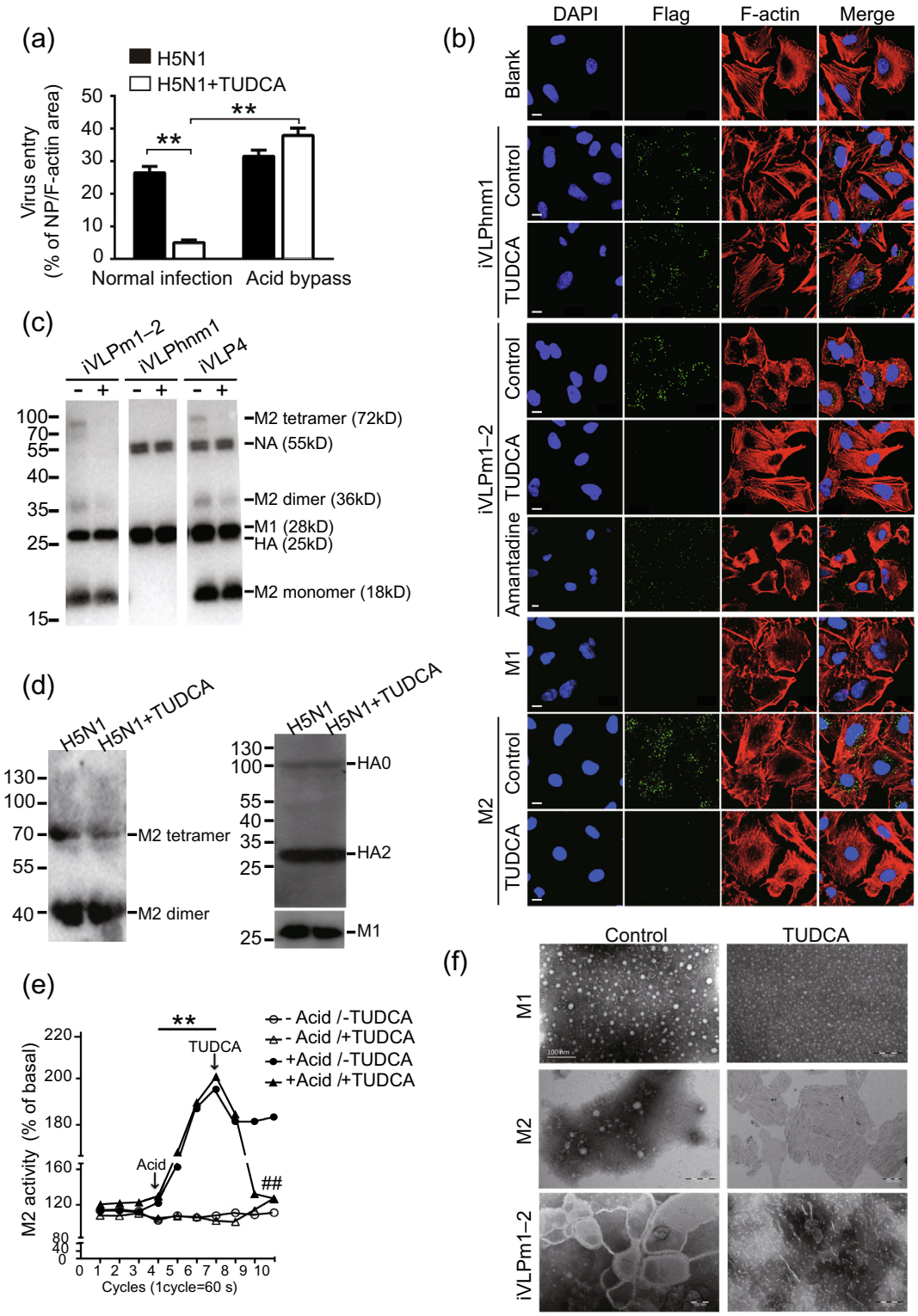

Fig. 3. TUDCA targets M2. (a) Internalization of H5N1 IAV after acid bypass assay, shown as percentage of NP positive staining of total cell area obtained from confocal observations, **, $P \leq 0.01$. (b) Confocal observations of iVLPhnm1, iVLPm1–2, M1 and M2 uptake into A549 cells compared with Blank, in the absence (Control) or presence (TUDCA) of TUDCA, or 100 μmol/L amantadine. Flag indicating internalized proteins stained in green, F-actin in red and nuclei with DAPI in blue, scale bar: 10 μm (c, d) TUDCA disrupts M2 oligomers of iVLPs; (c) and authentic H5N1 IAV (d) using western blot. (e) M2 activity measured with iVLPm1–2. Values were normalized to the basal non-activated fluorescence of each trace and shown as percentage of basal levels. **, $P \leq 0.01$, acid stimulation *vs.* non-acid-stimulated; ##, $P \leq 0.01$, TUDCA vs. non-TUDCA-treated. (f) TEM observations of M1, M2 and iVLPm1–2 in the absence (Control) or presence of TUDCA.

brane deformation [35]. In this regard, it is plausible that AH of M2 utilizes a similar mechanism triggering IAV entry by inducing membrane curvature. However, due to being interior of IAV, it is more likely that AH of M2 reinforces the contact between the viral envelope and host membrane by a protruding viral envelope. The implication of M2 as CPP is by far not fully defined and additional

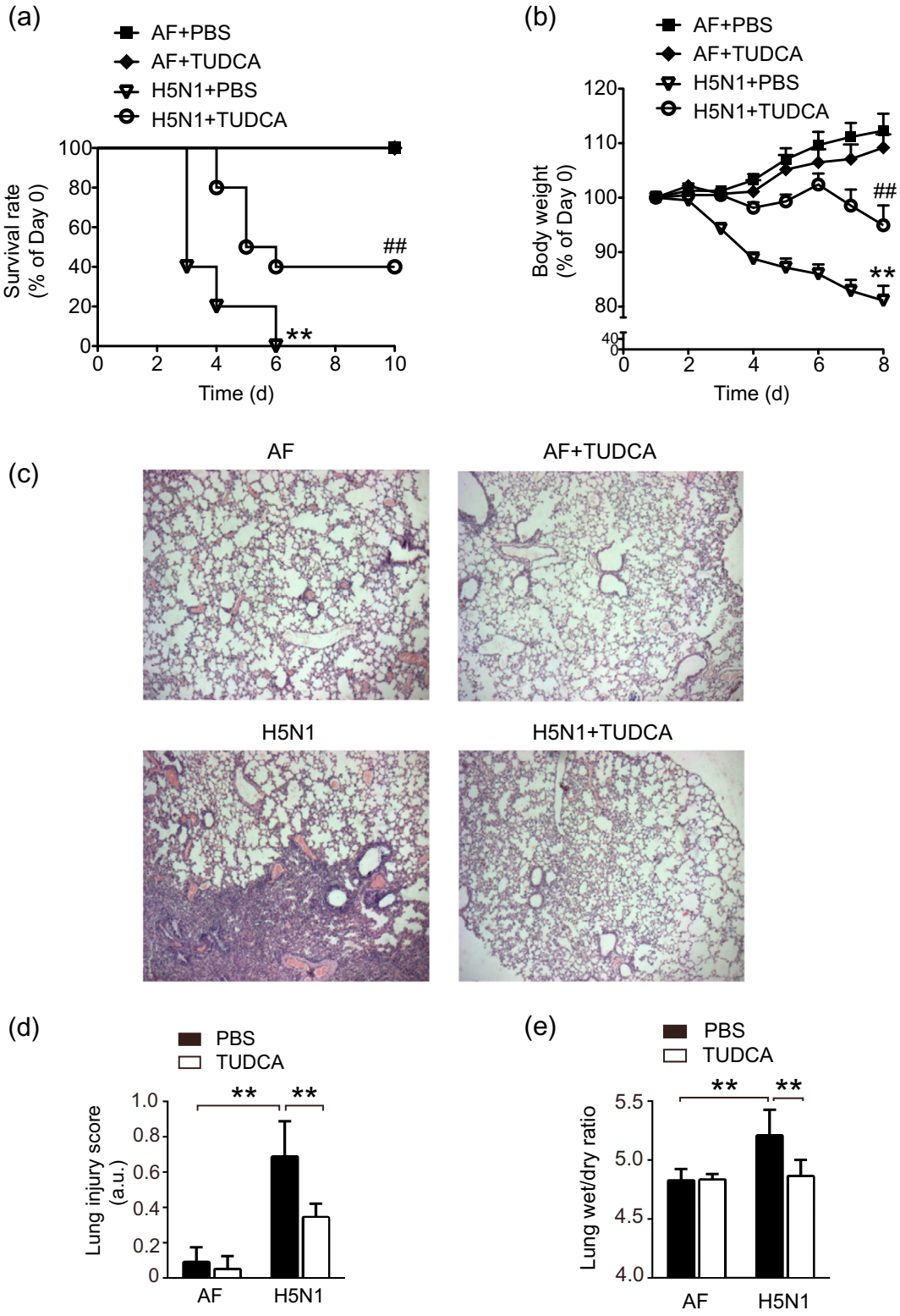

Fig. 4. In vivo anti-H5N1 effects of TUDCA. (a) Survival rate and (b) body weight of experimental mice after intratracheal instillation of vehicle control (AF) or H5N1 IAV with or without intraperitoneal injection of TUDCA (150 mg/kg) 6 and 24 h before infection. **, $P \leq 0.01$ *vs.* AF + PBS; ##, $P \leq 0.01$ *vs.* H5N1 + PBS. (c, d) H&E staining of mouse lung tissue (c) and corresponding lung injury score (d). (e) Pulmonary edema evaluated as wet/dry ratio. **, $P \leq 0.01$.

work will be required to understand whether the CPP property of M2 is the nature of IAV entry.

Besides cell-penetration, AH that is positively charged could be attracted by negatively charged BA. BA are facial amphiphiles, adopting an almost flat conformation with a rigid steroidal backbone in parallel with the interface, which allows contact of hydroxyl groups with the aqueous environment [36]. Typically, conjugated head groups of BAs are able to capture cationic species

[37]. Our TEM and AFM data (Figs. 3f and S3f, g (online)) suggest that TUDCA may form a complex with M2, which inherited the flat conformation of BA. This complex may be composed of a hydrophobic interface of BA in parallel with a hydrophilic contact *via* electrostatic forces between positively charged M2 AH and negatively charged TUDCA. Thus, TUDCA reorganization of the M2 protein deforms the liposomal construct of iVLPm1–2, shown as strings of membranous debris. As binding features of BA usually appear above millimolar concentrations [37], this may explain the high doses of TUDCA required in this study.

Taken together, we identified an alternative antiviral role of TUDCA. Rather than modulating the UPR of host cells, disrupting viral proton channel M2 may mediate the anti-IAV effect of TUDCA. Application of this class of inhibitors will unravel previously unidentified but important mechanisms to expand our understanding of IAV biology. As TUDCA is a clinically available medication for liver disorders and currently under clinical evaluation for metabolic syndromes, its antiviral potential to repurpose an existing pharmacological treatment may complement the current anti-IAV arsenal.

Conflict of interest

The authors declare that they have no conflict of interest.

Acknowledgments

This work was supported by the National Natural Science Foundation of China (81788101, 81573587 and 81490531), the Ministry of Science and Technology of China (2015CB5534/6), 111 project (B08007), the Peking Union Medical College Youth Fund, and Fundamental Research Funds for Central Universities (3332013132), and the CAMS Innovation Fund for Medical Sciences (2017-I2M-1-009).

Appendix A. Supplementary data

Supplementary data associated with this article can be found, in the online version, at https://doi.org/10.1016/j.scib.2018.08.013.

References

[1] Taubenberger JK, Kash JC. Influenza virus evolution, host adaptation, and pandemic formation. Cell Host Microbe 2010;7:440–51.
[2] Herfst S, Schrauwen EJ, Linster M, et al. Airborne transmission of influenza a/h5n1 virus between ferrets. Science 2012;336:1534–41.
[3] de Jong MD, Simmons CP, Thanh TT, et al. Fatal outcome of human influenza a (h5n1) is associated with high viral load and hypercytokinemia. Nat Med 2006;12:1203–7.
[4] Edinger TO, Pohl MO, Stertz S. Entry of influenza a virus: host factors and antiviral targets. J General Virol 2014;95:263–77.
[5] Skehel JJ, Wiley DC. Receptor binding and membrane fusion in virus entry: the influenza hemagglutinin. Annu Rev Biochem 2000;69:531–69.
[6] Stauffer S, Feng Y, Nebioglu F, et al. Stepwise priming by acidic ph and a high K^+ concentration is required for efficient uncoating of influenza a virus cores after penetration. J Virol 2014;88:13029–46.
[7] Shulman NS, Kassaye SG, Winters MA, et al. More on the treatment-tropism relationship: the impact of prior antiretroviral treatment on hiv coreceptor tropism among subjects entering aids clinical trials group 175. J Infectious Dis 2007;196:328–9.
[8] Sakaguchi T, Tu Q, Pinto LH, et al. The active oligomeric state of the minimalistic influenza virus m2 ion channel is a tetramer. Proc Natl Acad Sci USA 1997;94:5000–5.
[9] Schnell JR, Chou JJ. Structure and mechanism of the m2 proton channel of influenza a virus. Nature 2008;451:591–5.
[10] Kawano K, Yano Y, Matsuzaki K. A dimer is the minimal proton-conducting unit of the influenza a virus m2 channel. J Mol Biol 2014;426:2679–91.
[11] Tobler K, Kelly ML, Pinto LH, et al. Effect of cytoplasmic tail truncations on the activity of the m(2) ion channel of influenza a virus. J Virol 1999;73:9695–701.
[12] Kochendoerfer GG, Salom D, Lear JD, et al. Total chemical synthesis of the integral membrane protein influenza a virus m2: role of its c-terminal domain in tetramer assembly. Biochemistry 1999;38:11905–13.
[13] Holsinger LJ, Nichani D, Pinto LH, et al. Influenza a virus m2 ion channel protein: a structure-function analysis. J Virol 1994;68:1551–63.
[14] Ekanayake EV, Fu R, Cross TA. Structural influences: cholesterol, drug, and proton binding to full-length influenza a m2 protein. Biophys J 2016;110:1391–9.
[15] Kim SS, Upshur MA, Saotome K, et al. Cholesterol-dependent conformational exchange of the c-terminal domain of the influenza a m2 protein. Biochemistry 2015;54:7157–67.
[16] Nguyen PA, Soto CS, Polishchuk A, et al. Ph-induced conformational change of the influenza m2 protein c-terminal domain. Biochemistry 2008;47:9934–6.
[17] Georgieva ER, Borbat PP, Norman HD, et al. Mechanism of influenza a m2 transmembrane domain assembly in lipid membranes. Sci Rep 2015;5:11757.
[18] de Aguiar Vallim TQ, Tarling EJ, Edwards PA. Pleiotropic roles of bile acids in metabolism. Cell Metab 2013;17:657–69.
[19] Boatright JH, Nicker son JM, Moring AG, et al. Bile acids in treatment of ocular disease. J Ocular Biol Dis Informatics 2009;2:149–59.
[20] Ozcan U, Yilmaz E, Ozcan L, et al. Chemical chaperones reduce er stress and restore glucose homeostasis in a mouse model of type 2 diabetes. Science 2006;313:1137–40.
[21] Yan H, Peng B, Liu Y, et al. Viral entry of hepatitis b and d viruses and bile salts transportation share common molecular determinants on sodium taurocholate cotransporting polypeptide. J Virol 2014;88:3273–84.
[22] Hassan IH, Zhang MS, Powers LS, et al. Influenza a viral replication is blocked by inhibition of the inositol-requiring enzyme 1 (ire1) stress pathway. J Biol Chem 2012;287:4679–89.
[23] Hrincius ER, Liedmann S, Finkelstein D, et al. Acute lung injury results from innate sensing of viruses by an er stress pathway. Cell Rep 2015;11:1591–603.
[24] Matute-Bello G, Downey G, Moore BB, et al. An official american thoracic society workshop report: features and measurements of experimental acute lung injury in animals. Am J Respir Cell Mol Biol 2011;44:725–38.
[25] Sulli C, Banik SS, Schilling J, et al. Detection of proton movement directly across viral membranes to identify novel influenza virus m2 inhibitors. J Virol 2013;87:10679–86.
[26] Banerjee I, Yamauchi Y, Helenius A, et al. High-content analysis of sequential events during the early phase of influenza a virus infection. PLoS One 2013;8:e68450.
[27] Desplanques AS, Nauwynck HJ, Vercauteren D, et al. Plasma membrane cholesterol is required for efficient pseudorabies virus entry. Virology 2008;376:339–45.
[28] Sun X, Whittaker GR. Role for influenza virus envelope cholesterol in virus entry and infection. J Virol 2003;77:12543–51.
[29] Fujioka Y, Tsuda M, Nanbo A, et al. A Ca^{2+}dependent signalling circuit regulates influenza a virus internalization and infection. Nat Commun 2013;4:2763.
[30] Bechara C, Sagan S. Cell-penetrating peptides: 20 years later, where do we stand? FEBS Lett 2013;587:1693–702.
[31] Guo Z, Peng H, Kang J, et al. Cell-penetrating peptides: possible transduction mechanisms and therapeutic applications. Biomed Rep 2016;4:528–34.
[32] Milletti F. Cell-penetrating peptides: classes, origin, and current landscape. Drug Discovery Today 2012;17:850–60.
[33] Claridge JK, Aittoniemi J, Cooper DM, et al. Isotropic bicelles stabilize the juxtamembrane region of the influenza m2 protein for solution nmr studies. Biochemistry 2013;52:8420–9.
[34] Rossman JS, Jing X, Leser GP, et al. Influenza virus m2 protein mediates escrt-independent membrane scission. Cell 2010;142:902–13.
[35] Shen H, Pirruccello M, De Camilli P. Snapshot: membrane curvature sensors and generators. Cell 2012;150:1300.
[36] Faustino C, Serafim C, Rijo P, et al. Bile acids and bile acid derivatives: use in drug delivery systems and as therapeutic agents. Expert Opin Drug Delivery 2016;13:1133–48.
[37] Thakur R, Das A, Adhikari C, et al. Partitioning of prototropic species of an anticancer drug ellipticine in bile salt aggregates of different head groups and hydrophobic skeletons: a photophysical study to probe bile salts as multisite drug carriers. Phys Chem Chem Phys 2014;16:15681–91.

Ning Li is an associate Professor at China Academy of Chinese Medical Sciences. She has worked on gluco-lipo toxicity in type 2 diabetes during her M.D. and post-doctoral training in the Department of Cell Physiology and Metabolism, University of Geneva, Switzerland. Dr. Li's current research interests include metabolic control in aging-related diseases and molecular targeted therapy of Chinese herbal medicine.

Ningyi Jin, academician of Chinese Academy of Engineering, is a professor at the Institute of Military Veterinary Medicine, Academy of Military Medicine, and Academy of Military Sciences. Dr. Jin's research interests include the isolation, identification, characteristics of virus and related mechanisms of infection and pathogenesis of virus; viral etiology, epidemiological law, distribution and harmfulness of viral diseases, early warning and scientific prevention and control of viral diseases; virus detection technology, early diagnosis and rapid detection of virus diseases; vaccine preparation technology platform, and genetically engineered vaccines and drugs.

Chengyu Jiang, is a professor and Executive Vice Dean of School of Basic Medicine at Peking Union Medical College and Chinese Academy of Medical Sciences. Her research is to elucidate molecular pathogenesis of Acute Respiratory Distress Syndrome induced by RNA viruses such as SARS-CoV, Avian and Swine Influenza, and Ebola. Dr. Jiang has proposed a number of repurposing drugs after elucidation of disease molecular targets.